

# MESON WAVE FUNCTIONS FROM HOLOGRAPHIC QCD AND THE ROLE OF INFRARED RENORMALONS IN PROTON-PROTON COLLISIONS

A. I. Ahmadov<sup>1,2</sup> \*, C. Aydin<sup>1</sup> †, and F. Keskin<sup>1</sup> ‡

<sup>1</sup> *Department of Physics, Karadeniz Technical University, 61080, Trabzon, Turkey*

<sup>2</sup> *Department of Theoretical Physics, Baku State University,  
Z. Khalilov st. 23, AZ-1148, Baku, Azerbaijan*

## Abstract

We calculate the contribution of the higher twist Feynman diagrams to the large- $p_T$  inclusive pion production cross section in proton-proton collisions in the case of the running and frozen coupling approaches within holographic QCD. The structure of infrared renormalon singularities of the higher twist subprocess cross section and its resummed expression are found. We compare the resummed higher twist cross sections with the ones obtained in the framework of the frozen coupling approximation and leading twist cross section. We discuss the phenomenological consequences of possible higher-twist contributions to the pion production in proton-proton collisions within holographic QCD.

PACS numbers: 12.38.-t, 13.60.Le, 14.40.Aq, 13.87.Fh,

Keywords: higher twist, holographic QCD, infrared renormalons,

---

\* E-mail: ahmadovazar@yahoo.com

† E-mail: coskun@ktu.edu.tr

‡ E-mail: feridunkeskin@ktu.edu.tr

## I. INTRODUCTION

One of the most interesting new developments in hadron physics is the application of the AdS/CFT correspondence [1] to nonperturbative QCD problems [2–8]. It is well known that AdS/CFT gives an important insight into the viscosity and other global properties of the hadronic system formed in heavy ion collisions [9]. The essential ansatz for the application of AdS/CFT to hadron physics is the indication that the QCD coupling  $\alpha_s(Q^2)$  becomes large. Therefore conformal symmetry can be applied to, for example solutions of the QCD Dyson Schwinger equations and phenomenological studies of QCD couplings based on physical observables such as  $\tau$  decay and the Bjorken sum rule show that the QCD  $\beta$  function vanishes and  $\alpha_s(Q^2)$  become constant at small virtuality; i.e., effective charges develop an infrared fixed point. Fully exploiting the gauge/gravity correspondence to produce a model for real strong interaction physics- a method called "holographic QCD" or "AdS/QCD"-may be attempted either through a top-down approach starting with a particular string theory and choosing a background that naturally produces QCD-like properties, or a bottom-up approach starting with real QCD properties and using them to obtain constraints on viable dual gravity theories.

The first attempts have been made for constructing phenomenological holographic models of QCD [4]. Surprisingly simple models consisting of gauge theory in an anti-de-Sitter space interval have turned out to provide a remarkably good description of the meson sector of QCD. Therefore, it will be interesting that the calculation of the higher twist effects within holographic QCD in proton-proton collisions in the running coupling approach.

The large-order behavior of a perturbative expansion in gauge theories is inevitably dominated by the factorial growth of renormalon diagrams [10–13]. In the case of quantum chromodynamics (QCD), the coefficients of perturbative expansions in the QCD coupling  $\alpha_s$  can increase dramatically even at low orders. This fact, together with the apparent freedom in the choice of renormalization scheme and renormalization scales, limits the predictive power of perturbative calculations, even in applications involving large momentum transfer, where  $\alpha_s$  is effectively small.

In this work we apply the running coupling approach [14] in order to compute the effects of the infrared renormalons on the pion production in proton-proton collisions within holographic QCD. This approach was also employed previously [15–18] to calculate the inclusive

meson production in proton-proton and photon-photon collisions.

For the calculations of the higher-twist cross sections on the dependence of wave functions of pion, we used the holographic QCD prediction  $\Phi_{hol}(x)$  [19–21] and pion asymptotic wave functions  $\Phi_{asy}(x)$  [22] from the perturbative QCD evolution. Theoretically obtained predicted results within holographic QCD were compared with results of the perturbative QCD which obtained by the running coupling and frozen coupling constants approaches.

The frozen coupling constant approach in Refs. [23–26] was used for calculation of integrals, such as

$$I \sim \int \frac{\alpha_s(Q^2)\Phi(x, Q^2)}{1-x} dx. \quad (1.1)$$

It should be noted that, in pQCD calculations, the argument of the QCD coupling constant (or the renormalization and factorization scale)  $Q^2$  should be taken equal to the square of the momentum transfer of a hard gluon in a corresponding Feynman diagram. But definition of  $\alpha_s(\hat{Q}^2)$  suffers from infrared singularities. Therefore, in the soft regions as  $x_1 \rightarrow 0$ , and  $x_2 \rightarrow 0$ , integrals (1.1) diverge and for their calculation some regularization methods are needed for  $\alpha_s(Q^2)$  in these regions. Investigation of the infrared renormalon effects in various inclusive and exclusive processes is one of the most important and interesting problem in the perturbative QCD. It is known that infrared renormalons are responsible for factorial growth of coefficients in perturbative series for the physical quantities. But, these divergent series can be resummed by means of the Borel transformation [10] and the principal value prescription [27]. Studies of higher-twist and renormalon effects also opened new prospects for evaluation of power suppressed corrections to processes characteristics.

We organize the paper as the follows. In Section II, we provide some formulas for the calculation of the contributions of the higher twist and leading twist diagrams. In Section III, we present the formulas and analysis of the higher-twist effects on the dependence of the pion wave function by the running coupling constant approach, and in Section IV, the numerical results for the cross section and discuss the dependence of the cross section on the pion wave functions are presented. Finally, some concluding remark are stated in Section V.

## II. HIGHER TWIST AND LEADING TWIST CONTRIBUTIONS TO INCLUSIVE REACTIONS

The higher-twist Feynman diagrams, which describe the subprocess  $q_1 + \bar{q}_2 \rightarrow \pi^+(\pi^-) + \gamma$  for the pion production in the proton-proton collision are shown in Fig.1. The amplitude for this subprocess can be found by means of the Brodsky-Lepage formula [28]

$$M(\hat{s}, \hat{t}) = \int_0^1 dx_1 \int_0^1 dx_2 \delta(1 - x_1 - x_2) \Phi_\pi(x_1, x_2, Q^2) T_H(\hat{s}, \hat{t}; x_1, x_2). \quad (2.1)$$

In Eq.(2.1),  $T_H$  is the sum of the graphs contributing to the hard-scattering part of the subprocess.

The Mandelstam invariant variables for subprocesses  $q_1 + \bar{q}_2 \rightarrow \pi^+(\pi^-) + \gamma$  are defined as

$$\hat{s} = (p_1 + p_2)^2, \quad \hat{t} = (p_1 - p_\pi)^2, \quad \hat{u} = (p_1 - p_\gamma)^2. \quad (2.2)$$

The pion wave functions predicted by AdS/QCD [19–21] and the PQCD evolution [22] has the form:

$$\begin{aligned} \Phi_{asy}^{hol}(x) &= \frac{4}{\sqrt{3}\pi} f_\pi \sqrt{x(1-x)}, \\ \Phi_{VSBGL}^{hol}(x) &= \frac{A_1 k_1}{2\pi} \sqrt{x(1-x)} \exp\left(-\frac{m^2}{2k_1^2 x(1-x)}\right), \quad \Phi_{asy}^p(x) = \sqrt{3} f_\pi x(1-x) \end{aligned} \quad (2.3)$$

where  $f_\pi$  is the pion decay constant.

The cross section for the higher-twist subprocess  $q_1 \bar{q}_2 \rightarrow \pi^+(\pi^-)\gamma$  is given by the expression

$$\frac{d\sigma}{d\hat{t}}(\hat{s}, \hat{t}, \hat{u}) = \frac{8\pi^2 \alpha_E C_F}{27} \frac{[D(\hat{t}, \hat{u})]^2}{\hat{s}^3} \left[ \frac{1}{\hat{u}^2} + \frac{1}{\hat{t}^2} \right] \quad (2.4)$$

where

$$D(\hat{t}, \hat{u}) = e_1 \hat{t} \int_0^1 dx \left[ \frac{\alpha_s(Q_1^2) \Phi_\pi(x, Q_1^2)}{1-x} \right] + e_2 \hat{u} \int_0^1 dx \left[ \frac{\alpha_s(Q_2^2) \Phi_\pi(x, Q_2^2)}{1-x} \right]. \quad (2.5)$$

In the Eq.(2.5)  $Q_1^2 = (x-1)\hat{u}$  and  $Q_2^2 = -x\hat{t}$  represent the momentum squared carried by the hard gluon in Fig.1,  $e_1(e_2)$  is the charge of  $q_1(\bar{q}_2)$  and  $C_F = \frac{4}{3}$ . The higher-twist contribution to the large- $p_T$  pion production cross section in the process  $pp \rightarrow \pi^+(\pi^-) + \gamma + X$  is [29, 30]

$$\Sigma_M^{HT} \equiv E \frac{d\sigma}{d^3p} = \int_0^1 \int_0^1 dx_1 dx_2 G_{q_1/h_1}(x_1) G_{q_2/h_2}(x_2) \frac{\hat{s}}{\pi} \frac{d\sigma}{d\hat{t}}(q\bar{q} \rightarrow \pi\gamma) \delta(\hat{s} + \hat{t} + \hat{u}). \quad (2.6)$$

We denote the higher-twist cross section obtained using the frozen coupling constant approach by  $(\Sigma_\pi^{HT})^0$ .

Regarding the higher-twist corrections to the pion production cross section, a comparison of our results with leading-twist contributions is crucial. We take two leading-twist subprocesses for the pion production: (1) quark-antiquark annihilation  $q\bar{q} \rightarrow g\gamma$ , in which the  $g \rightarrow \pi^+(\pi^-)$  and (2) quark-gluon fusion,  $qg \rightarrow q\gamma$ , with subsequent fragmentation of the final quark into a meson,  $q \rightarrow \pi^+(\pi^-)$  [15, 17].

### III. THE HIGHER TWIST MECHANISM IN HOLOGRAPHIC QCD AND INFRARED RENORMALONS

The main problem in our investigation is the calculation of integral in (2.5) by the running coupling constant approach within holographic QCD and also discussion of the problem of normalization of the higher twist process cross section in the context of the same approach. Therefore, it is worth noting that, the renormalization scale (argument of  $\alpha_s$ ) according to Fig.1 should be chosen equal to  $Q_1^2 = (x-1)\hat{u}$ ,  $Q_2^2 = -x\hat{t}$ . The integral in Eq.(2.5) in the framework of the running coupling approach takes the form

$$I(\mu_{R_0}^2) = \int_0^1 \frac{\alpha_s(\lambda\mu_{R_0}^2)\Phi_M(x, \mu_F^2)dx}{1-x}. \quad (3.1)$$

The  $\alpha_s(\lambda\mu_{R_0}^2)$  has the infrared singularity at  $x \rightarrow 1$ , for  $\lambda = 1-x$  or  $x \rightarrow 0$ , for  $\lambda = x$  and so the integral (3.1) diverges. For the regularization of the integral, we express the running coupling at scaling variable  $\alpha_s(\lambda\mu_{R_0}^2)$  with the aid of the renormalization group equation in terms of the fixed one  $\alpha_s(Q^2)$ . The solution of renormalization group equation for the running coupling  $\alpha \equiv \alpha_s/\pi$  has the form [27]

$$\frac{\alpha(\lambda)}{\alpha} = \left[1 + \alpha \frac{\beta_0}{4} \ln \lambda\right]^{-1}. \quad (3.2)$$

Then, for  $\alpha_s(\lambda Q^2)$ , we get

$$\alpha(\lambda Q^2) = \frac{\alpha_s}{1 + \ln \lambda/t} \quad (3.3)$$

where  $t = 4\pi/\alpha_s(Q^2)\beta_0 = 4/\alpha\beta_0$ .

Having inserted Eq.(3.3) into Eq.(2.5) we obtain

$$D(\hat{t}, \hat{u}) = e_1 \hat{t} \int_0^1 dx \frac{\alpha_s(\lambda\mu_{R_0}^2)\Phi_M(x, Q_1^2)}{1-x} + e_2 \hat{u} \int_0^1 dx \frac{\alpha_s(\lambda\mu_{R_0}^2)\Phi_M(x, Q_2^2)}{1-x}$$

$$= e_1 \hat{t} \alpha_s(-\hat{u}) t_1 \int_0^1 dx \frac{\Phi_M(x, Q_1^2)}{(1-x)(t_1 + \ln \lambda)} + e_2 \hat{u} \alpha_s(-\hat{t}) t_2 \int_0^1 dx \frac{\Phi_M(x, Q_2^2)}{(1-x)(t_2 + \ln \lambda)} \quad (3.4)$$

where  $t_1 = 4\pi/\alpha_s(-\hat{u})\beta_0$  and  $t_2 = 4\pi/\alpha_s(-\hat{t})\beta_0$ .

Although the integral (3.4) is still divergent, it is recast into a suitable form for calculation. Making the change of variable as  $z = \ln \lambda$ , we obtain

$$D(\hat{t}, \hat{u}) = e_1 \hat{t} \alpha_s(-\hat{u}) t_1 \int_0^1 dx \frac{\Phi_M(x, Q_1^2)}{(1-x)(t_1 + z)} + e_2 \hat{u} \alpha_s(-\hat{t}) t_2 \int_0^1 dx \frac{\Phi_M(x, Q_2^2)}{(1-x)(t_2 + z)} \quad (3.5)$$

In order to calculate (3.5) we will apply the integral representation of  $1/(t+z)$  [31, 32].

$$\frac{1}{(t+z)} = \int_0^\infty e^{-(t+z)u} du, \quad (3.6)$$

gives

$$D(\hat{t}, \hat{u}) = e_1 \hat{t} \alpha_s(-\hat{u}) t_1 \int_0^1 \int_0^\infty \frac{\Phi_\pi(x, Q_1^2) e^{-(t_1+z)u} du dx}{(1-x)} + e_2 \hat{u} \alpha_s(-\hat{t}) t_2 \int_0^1 \int_0^\infty \frac{\Phi_\pi(x, Q_2^2) e^{-(t_2+z)u} du dx}{(1-x)} \quad (3.7)$$

In the case  $\Phi_{asy}^{hol}(x)$  for the  $D(\hat{t}, \hat{u})$  it is written as

$$D(\hat{t}, \hat{u}) = \frac{16f_\pi e_1 \hat{t}}{\sqrt{3}\beta_0} \int_0^\infty du e^{-t_1 u} B\left(\frac{3}{2}, \frac{1}{2} - u\right) + \frac{16f_\pi e_2 \hat{u}}{\sqrt{3}\beta_0} \int_0^\infty du e^{-t_2 u} B\left(\frac{3}{2}, \frac{1}{2} - u\right) \quad (3.8)$$

and for  $\Phi_{asy}^p(x)$  wave function

$$D(\hat{t}, \hat{u}) = \frac{4\sqrt{3}\pi f_\pi e_1 \hat{t}}{\beta_0} \int_0^\infty du e^{-t_1 u} \left[ \frac{1}{1-u} - \frac{1}{2-u} \right] + \frac{4\sqrt{3}\pi f_\pi e_2 \hat{u}}{\beta_0} \int_0^\infty du e^{-t_2 u} \left[ \frac{1}{1-u} - \frac{1}{2-u} \right]. \quad (3.9)$$

where  $B(\alpha, \beta)$  is Beta function. The structure of the infrared renormalon poles in Eq.(3.8) and Eq.(3.9) strongly depend on the wave functions of the pion. To remove them from Eq.(3.8) and Eq.(3.9) we adopt the principal value prescription. We denote the higher-twist cross section obtained using the running coupling constant approach by  $(\Sigma_\pi^{HT})^{res}$ .

#### IV. NUMERICAL RESULTS AND DISCUSSION

In this section, we discuss the higher-twist contributions calculated in the context of the running and frozen coupling constant approaches on the dependence of the chosen pion wave functions in the process  $pp \rightarrow \pi^+ (or \pi^-) \gamma + X$ . In numerical calculations for the quark distribution function inside the proton, the MSTW distribution function [33], and the gluon and quark fragmentation [34] functions into a pion have been used. The results of our

numerical calculations are displayed in Figs.2-14. Firstly, it is very interesting comparing the higher-twist cross sections obtained within holographic QCD with the ones obtained within perturbative QCD. In Fig.2 and Fig.3 we show the dependence of higher-twist cross sections  $(\Sigma_{\pi^+}^{HT})^0$ ,  $(\Sigma_{\pi^+}^{HT})^{res}$  calculated in the context of the frozen and running coupling constant approaches as a function of the pion transverse momentum  $p_T$  for different pion wave functions at  $y = 0$ . It is seen from Fig.2 and Fig.3 that the higher-twist cross section is monotonically decreasing with an increase in the transverse momentum of the pion. In Fig.4- Fig.7, we show the dependence of the ratios  $(\Sigma_{HT}^{hol})/(\Sigma_{HT}^p)$ ,  $(\Sigma_{\pi}^{HT})^{res}/(\Sigma_{\pi^+}^{HT})^0$ ,  $(\Sigma_{\pi^+}^{HT})^0/(\Sigma_{\pi^+}^{LT})$  and  $(\Sigma_{\pi^+}^{HT})^{res}/(\Sigma_{\pi^+}^{LT})$  as a function of the pion transverse momentum  $p_T$  for  $\Phi_{\pi}^{hol}(x)$ ,  $\Phi_{\pi}^p(x)$  and  $\Phi_{VSBGL}^{hol}(x)$  pion wave functions. Here  $\Sigma_{\pi^+}^{LT}$  is the leading-twist cross section, respectively. As shown in Fig.4, in the region  $2 \text{ GeV}/c < p_T < 30 \text{ GeV}/c$  resummed higher-twist cross section for  $\Phi_{\pi}^{hol}(x)$  is suppress by about half orders of magnitude relative to the resummed higher-twist cross section for  $\Phi_{\pi}^p(x)$  also higher-twist cross section for  $\Phi_{\pi}^p(x)$  is suppress by about half orders of magnitude relative to the higher-twist cross section for  $\Phi_{VSBGL}^{hol}(x)$ . In Fig.5 and Fig.6, we show the dependence of the ratios  $(\Sigma_{\pi}^{HT})^{res}/(\Sigma_{\pi^+}^{HT})^0$ , and  $(\Sigma_{\pi^+}^{HT})^0/(\Sigma_{\pi^+}^{LT})$  as a function of the meson transverse momentum  $p_T$  for the  $\Phi_{\pi}^{hol}(x)$ ,  $\Phi_{\pi}^p(x)$  and  $\Phi_{VSBGL}^{hol}(x)$  pion wave functions. It is observed from Fig.5 that, the ratios for all wave functions decrease with an increase in the transverse momentum of pion, but in the region  $2 \text{ GeV}/c < p_T < 8 \text{ GeV}/c$  resummed higher-twist cross section for  $\Phi_{\pi}^{hol}(x)$  is suppress by about 2-3 and 2-4 orders of magnitude relative to the higher-twist cross sections calculated in the context of the frozen coupling method for  $\Phi_{\pi}^p(x)$  and  $\Phi_{VSBGL}^{hol}(x)$ , respectively. Also, resummed higher-twist cross section for  $\Phi_{\pi}^p(x)$  is suppress by about 1-3 orders of magnitude relative to the higher-twist cross sections calculated in the context of the frozen coupling method for  $\Phi_{VSBGL}^{hol}(x)$ . But, as shown in Fig.6, the ratios decrease with increasing in the  $p_T$  transverse momentum of the pion and has a minimum approximately at the point  $p_T = 13 \text{ GeV}/c$ , then the ratios increase with increasing in the  $p_T$  transverse momentum of the pion. In Fig.7 is similar to Fig.6 with an exception that there in a minimum approximately at the point  $p_T = 25 \text{ GeV}/c$ . In Fig.8 - Fig.10, we have depicted higher-twist cross sections  $(\Sigma_{\pi^+}^{HT})$ , and ratio  $(\Sigma_{HT}^{hol})/(\Sigma_{HT}^p)$ , as a function of the rapidity  $y$  of the pion at  $\sqrt{s} = 62.4 \text{ GeV}$  and  $p_T = 4.9 \text{ GeV}/c$ . Figures show that higher-twist cross section and ratios have a different distinctive. The resummed higher-twist cross section for  $\Phi_{\pi}^{hol}(x)$  has a maximum approximately at the point  $y = -1.92$ . However in this point higher-twist cross section for  $\Phi_{VSBGL}^{hol}(x)$  has a minimum. As shown in

Fig.9 in the region  $(-2.52 \leq y \leq -1.92)$  the ratios  $(\Sigma_{HT}^{hol})^0/(\Sigma_{HT}^p)^0$  and  $(\Sigma_{VSBGL}^{hol})^0/(\Sigma_{HT}^p)^0$  increase with an increase of the  $y$  rapidity of the pion and has a maximum approximately at the point  $y = 1.22$ , but ratio  $(\Sigma_{HT}^{hol})^0/(\Sigma_{VSBGL}^{hol})^0$  has a minimum in this point. As is seen from Fig.10 ratios  $R = (\Sigma_{\pi^+}^{HT})^{res}/(\Sigma_{\pi^+}^{HT})^0$ , for all wave functions increase with an increase of the  $y$  rapidity of the pion and has a maximum approximately at the point  $y = -1.92$ . In the region  $-2.52 < y < -1.92$  resummed higher-twist cross section is suppress by about half order of magnitude relative to the higher-twist cross section calculated in the framework of the frozen coupling approach. Besides that, the ratio decreases with an increase in the  $y$  rapidity of the pion. As is seen from Fig.10, the ratio  $R$  depends on the choice of the pion wave function. Analysis of our calculations shows that  $(\Sigma_{\pi^+}^{HT})^0$ ,  $(\Sigma_{\pi^+}^{HT})^{res}$  higher-twist cross sections and ratio sensitive to pion wave functions predicted holographic and perturbative QCD.

We have also carried out comparative calculations in the center-of-mass energy  $\sqrt{s} = 200 \text{ GeV}$  and obtained results are displayed in Fig.11-Fig.14. Analysis of our calculations at the center-of-mass energies  $\sqrt{s} = 62.4 \text{ GeV}$  and  $\sqrt{s} = 200 \text{ GeV}$ , show that with increasing in the beam energy contributions of higher-twist effects to the cross section decrease by about one-two order. As is seen from Fig.5, Fig.7, Fig.10 and Fig.13 that infrared renormalon effects enhance the perturbative predictions for the pion production cross section in the proton-proton collisions about 2-3 order. This feature of infrared renormalons may help the explain theoretical interpretations with future experimental data for the pion production cross section in the proton-proton collisions. In our calculations, the higher-twist cross section of the process the dependence of the transverse momentum of pion appears in the range of  $(10^{-8} \div 10^{-26}) \text{ mb/GeV}^2$ . Therefore, higher-twist cross section obtained in our work should be observable at RHIC.

## V. CONCLUSIONS

Proton-proton collisions are known to be the most elementary interactions and form the very basis of our knowledge about the nature of high energy collisions in general. Physicists, by and large, hold the view quite firmly that the perturbative quantum-chromodynamics provides a general framework for the studies on high energy particle-particle collisions. Obviously, the unprecedented high energies attained at Large Hadron



Collider offer new window and opportunities to test the proposed QCD dynamics with its pros and cons. However, we should remember that LHC opens a new kinematical regime at high energy, where several questions related to the description of the high-energy regime of the QCD. Consequently, studies of proton-proton interactions at the RHIC and LHC could provide valuable information on the QCD dynamics at high energies. In this work the single meson inclusive production via higher twist mechanism within holographic QCD are calculated. For calculation of the cross section, the running coupling constant approach is applied and infrared renormalon poles in the cross section expression are revealed. Infrared renormalon induced divergences is regularized by means of the principal value prescription and the resummed expression (the Borel sum) for the higher-twist cross section is found. It is observed that, the resummed higher-twist cross section differs considerably from that found using the frozen coupling approximation, in some region. The following results can be concluded from the experiments; the higher-twist contributions to single meson production cross section in the proton-proton collisions have important phenomenological consequences, the higher-twist pion production cross section in the proton-proton collisions depends on the form of the pion model wave functions and may be used for their study. Also the contributions of renormalons effects within holographic QCD in this process are essential and may help to analyse experimental results. Further investigations are needed in order to clarify the role of higher-twist effects in QCD. Especially, the forthcoming RHIC and LHC measurements will provide further tests of the dynamics of large- $p_T$  hadron production beyond the leading twist.

### Acknowledgments

One of author A.I.Ahmadov is grateful to all members of the Department of Physics of Karadeniz Technical University for appreciates hospitality extended to him in Trabzon. Financial support by TUBITAK under grant number 2221(Turkey) is also gratefully acknowledged.

- 
- [1] J. M. Maldacena, Adv. Theor. Math. Phys. 2, 231 (1998); Int. J. Theor. Phys. 38, 1113 (1999); S. S. Gubser, I. R. Klebanov and A. M. Polyakov, Phys. Lett. B 428, 105 (1998); E. Witten,

- Adv. Theor. Math. Phys. 2, 253 (1998).
- [2] J. Polchinski and M. J. Strassler, Phys. Rev. Lett. 88, 031601 (2002).
  - [3] R. A. Janik and R. Peschanski, Nucl. Phys. B 565, 193 (2000).
  - [4] J. Erlich, E. Katz, D. T. Son and M. A. Stephanov, Phys. Rev. Lett. 95, 261602 (2005) [arXiv:hep-ph/0501128].
  - [5] A. Karch, E. Katz, D. T. Son and M. A. Stephanov, Phys. Rev. D 74, 015005 (2006).
  - [6] S. J. Brodsky and G. F. de Teramond, Phys.Lett **B582**, 211 (2004).
  - [7] G. F. de Teramond and S. J. Brodsky, Phys. Rev. Lett. 94, 201601 (2005).
  - [8] G. F. de Teramond and S. J. Brodsky, Phys. Rev. Lett. 96, 201601 (2006).
  - [9] P. Kovtun, D. T. Son and A. O. Starinets, Phys. Rev. Lett. 94, 111601 (2005).
  - [10] G.'t. Hooft, in The Whys of Subnuclear Physics, Erice, 1977, edited by A. Zichichi (Plenum, New York, 1979), p.94
  - [11] A. H. Mueller, Nucl. Phys. **B250**, 327 (1985); Phys. Lett. **B308**, 355 (1993).
  - [12] V. I. Zakharov, Nucl. Phys. **B385**,452 (1992).
  - [13] M. Beneke, Phys. Rep. **317**, 1 (1999).
  - [14] S.S. Agaev, Phys. Lett. **B360**, 117 (1995); **B369**, 379(E) (1996).
  - [15] A. I. Ahmadov, Coskun Aydin, Sh. M. Nagiyev, Yilmaz A. Hakan, and E. A. Dadashov, Phys. Rev. **D80**, 016003 (2009).
  - [16] A. I. Ahmadov, Coskun Aydin, E. A. Dadashov and Sh. M. Nagiyev, Phys. Rev. **D81**, 054016 (2010).
  - [17] A. I. Ahmadov, R. M. Burjaliyev, Int. J. Mod. Phys. **E20**, 1243 (2011).
  - [18] A. I. Ahmadov, Sh. M. Nagiyev, and E. A. Dadashov, Int. J. Mod. Phys. **E21**, 1250014 (2012).
  - [19] S. J. Brodsky and G. F. de Teramond, Phys. Rev. **D77**, 056007 (2008).
  - [20] S. J. Brodsky, arxiv:hep-ph/0707.2643.
  - [21] A. Vega, I. Schmidt, T. Branz, T.Gutsche,V. Lyubovitskij, Phys. Rev. **D80**, 055014 (2009).
  - [22] G. P. Lepage and S. J. Brodsky, Phys.Lett. **B87**, 359 (1979).
  - [23] A. I. Ahmadov, I. Boztosun, R. Kh. Muradov, A. Soylu, and E. A. Dadashov, Int. J. Mod.Phys. **E15**, 1209 (2006).
  - [24] A. I. Ahmadov, I. Boztosun, A. Soylu, and E. A. Dadashov, Int. J. Mod.Phys. **E17**, 1041 (2008).
  - [25] J. A. Bagger and J. F. Gunion, Phys. Rev. **D25**, 2287 (1982).

- [26] V. N. Baier and A. Grozin, Phys. Lett. **B96**, 181 (1980); S. Gupta, Phys. Rev. **D24**, 1169 (1981).
- [27] H. Contopanagos and G. Sterman, Nucl. Phys. **B419**, 77 (1994).
- [28] G. L. Lepage and S. J. Brodsky, Phys. Rev. **D22**, 2157 (1980).
- [29] J. F. Owens, Rev. Mod. Phys. **59**, 465 (1987).
- [30] W. Greiner, S. Schramm and E. Stein, Quantum Chromodynamics, 2nd edn.(Berlin, Springer, 2002), pp.551.
- [31] J. Zinn-Justin, Phys. Rept. **70**, 109 (1981).
- [32] A. Erdelyi, Higher Transcendental Functions (McGrow-Hill Book Company, New York, 1953), Vol.2.
- [33] A. D. Martin, W. J. Stirling, R. S. Thorne, and G. Watt, hep-ph/0901.0002.
- [34] S. Albino, B. A. Kniehl, G. Kramer, Nucl.Phys. **B725**, 181 (2005).

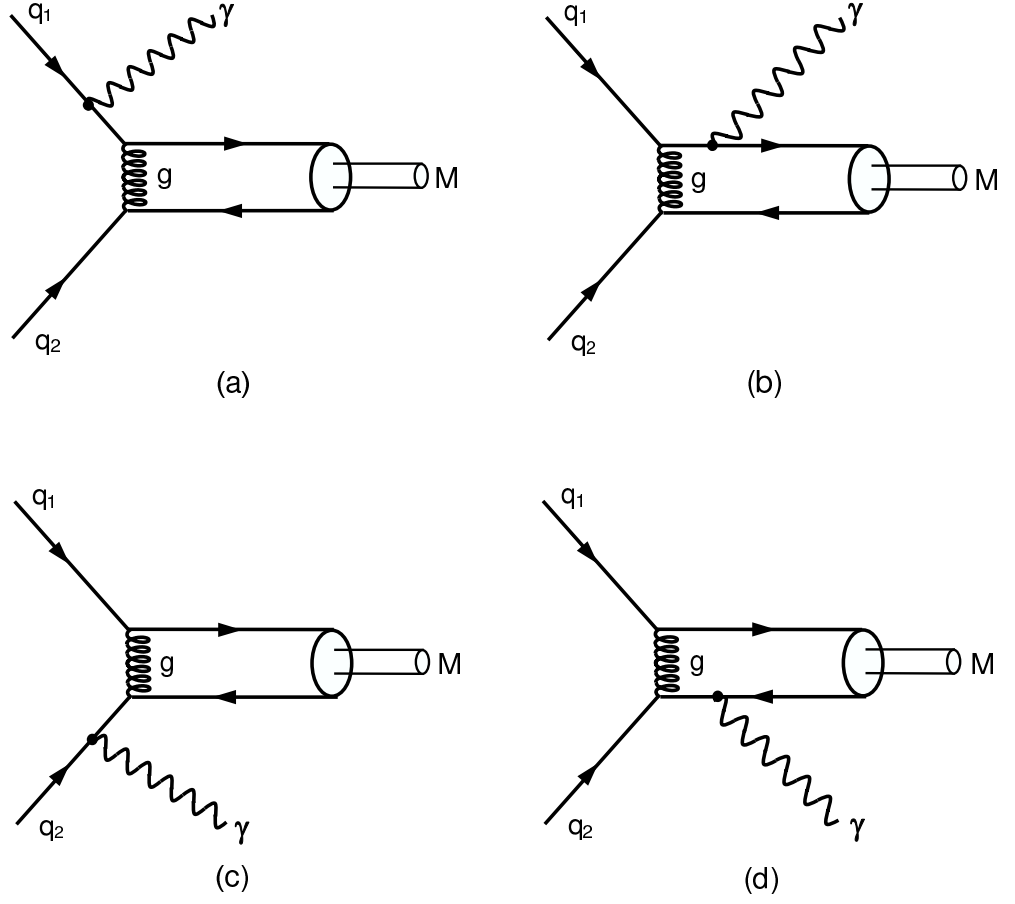


FIG. 1: Feynman diagrams for the higher twist subprocess,  $q_1 q_2 \rightarrow \pi^+ (\text{or } \pi^-) \gamma$ .

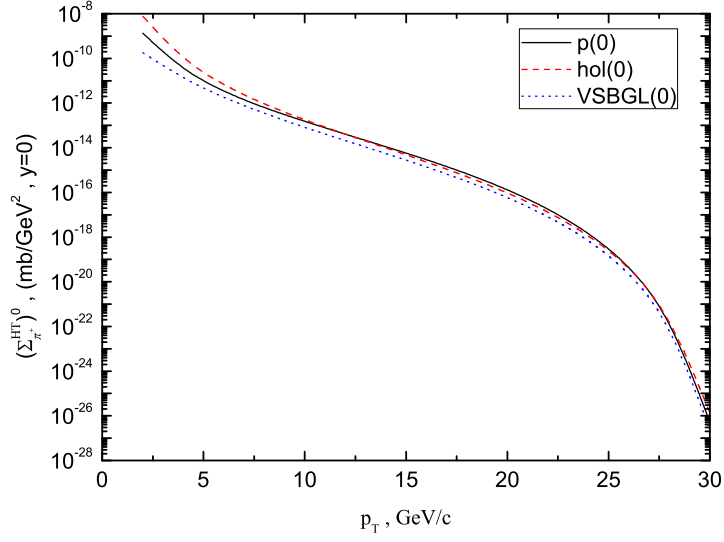


FIG. 2: Higher-twist  $\pi^+$  production cross section  $(\Sigma_{\pi^+}^{HT})^0$  as a function of the  $p_T$  transverse momentum of the pion at the c.m. energy  $\sqrt{s} = 62.4 \text{ GeV}$ .

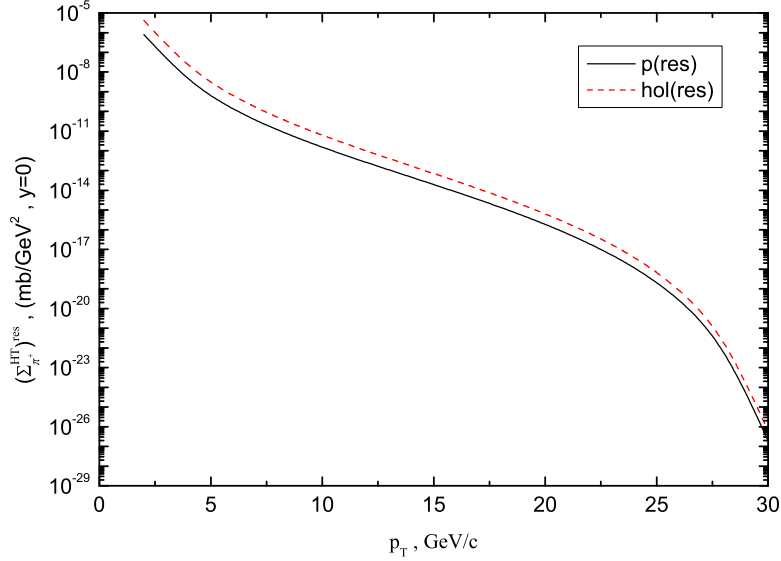


FIG. 3: Higher-twist  $\pi^+$  production cross section  $(\Sigma_{\pi^+}^{HT})^{res}$  as a function of the  $p_T$  transverse momentum of the pion at the c.m.energy  $\sqrt{s} = 62.4 \text{ GeV}$ .

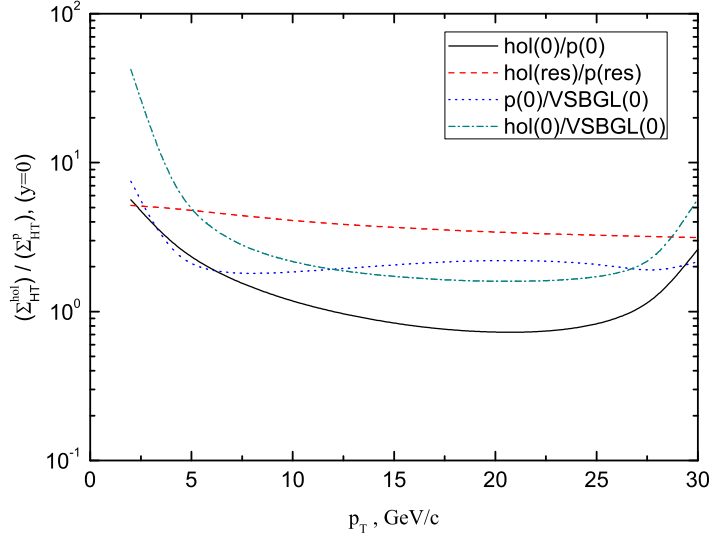


FIG. 4: Ratio  $(\Sigma_{HT}^{hol})/(\Sigma_{HT}^p)$ , where higher-twist contribution are calculated for the pion rapidity  $y = 0$  at the c.m.energy  $\sqrt{s} = 62.4 \text{ GeV}$  as a function of the pion transverse momentum,  $p_T$ .

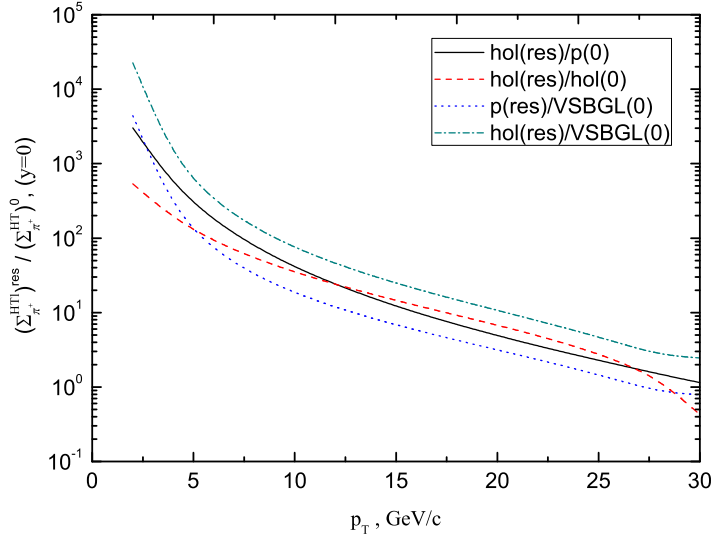


FIG. 5: Ratio  $(\Sigma_{\pi^+}^{HT})^{res}/(\Sigma_{\pi^+}^{HT})^0$ , as a function of the  $p_T$  transverse momentum of the pion at the c.m. energy  $\sqrt{s} = 62.4 \text{ GeV}$ .

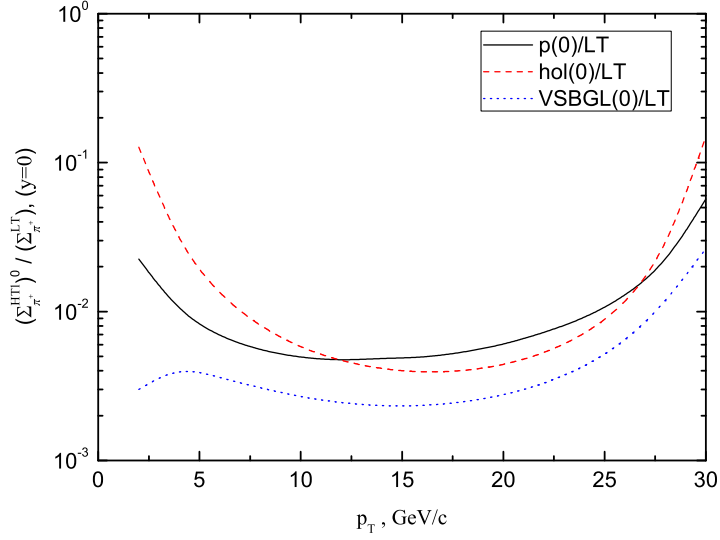


FIG. 6: Ratio  $(\Sigma_{\pi^+}^{HT})^0 / (\Sigma_{\pi^+}^{LT})^0$ , where higher-twist contribution are calculated for the pion rapidity  $y = 0$  at the c.m.energy  $\sqrt{s} = 62.4 \text{ GeV}$  as a function of the pion transverse momentum,  $p_T$ .

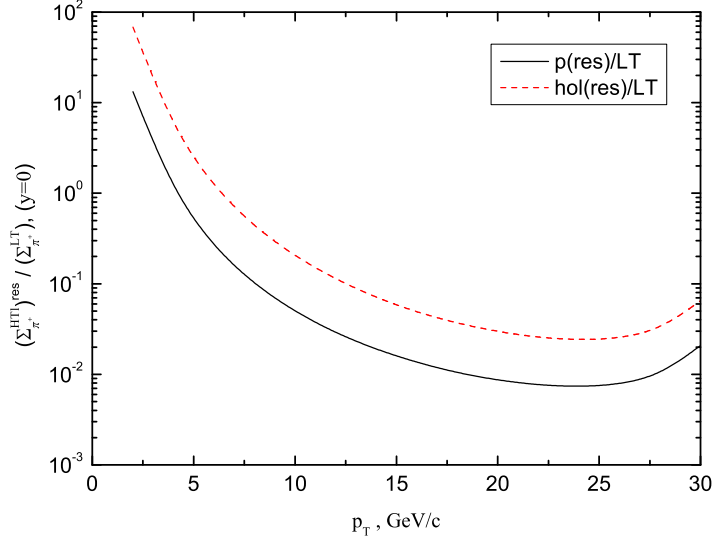


FIG. 7: Ratio  $(\Sigma_{\pi^+}^{HT})^{res} / (\Sigma_{\pi^+}^{LT})^0$ , as a function of the  $p_T$  transverse momentum of the pion at the c.m. energy  $\sqrt{s} = 62.4 \text{ GeV}$ .

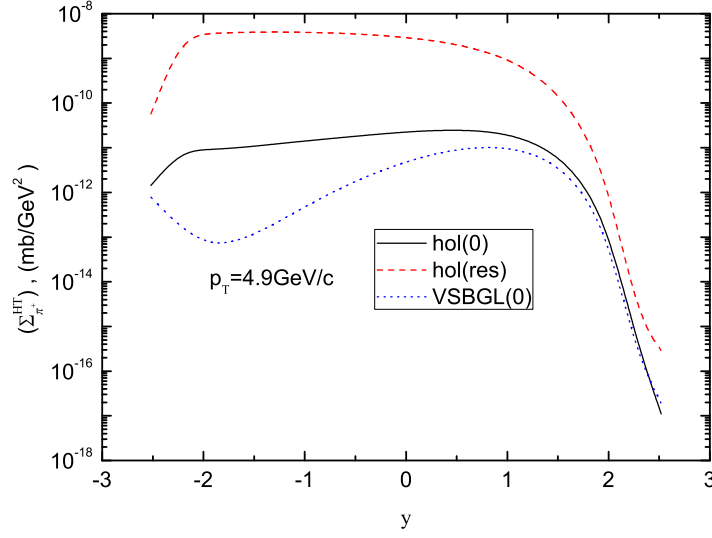


FIG. 8: Higher-twist  $\pi^+$  production cross section  $(\Sigma_{\pi^+}^{HT})$ , as a function of the  $y$  rapidity of the pion at the transverse momentum of the pion  $p_T = 4.9 \text{ GeV}/c$ , at the c.m. energy  $\sqrt{s} = 62.4 \text{ GeV}$ .

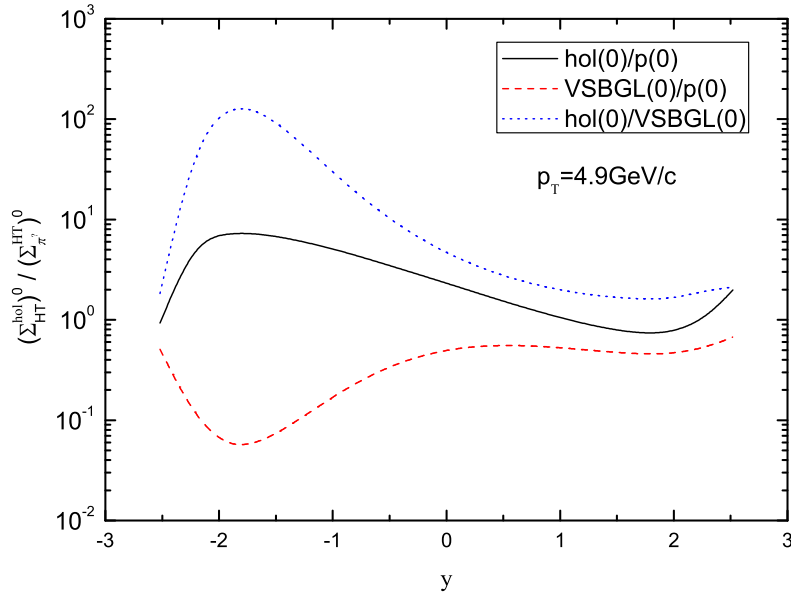


FIG. 9: Ratio  $(\Sigma_{HT}^{hol})^0/(\Sigma_{\pi^+}^{HT})^0$ , as a function of the  $y$  rapidity of the pion at the transverse momentum of the pion  $p_T = 4.9 \text{ GeV}/c$ , at the c.m. energy  $\sqrt{s} = 62.4 \text{ GeV}$ .



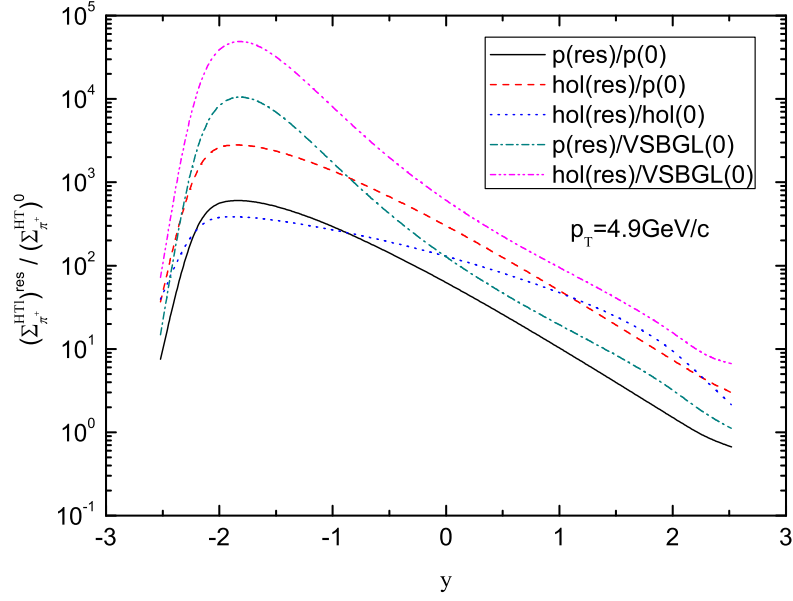


FIG. 10: Ratio  $(\Sigma_{\pi^+}^{HT})^{res}/(\Sigma_{\pi^+}^{HT})^0$ , as a function of the  $y$  rapidity of the pion at the transverse momentum of the pion  $p_T = 4.9 \text{ GeV}/c$ , at the c.m. energy  $\sqrt{s} = 62.4 \text{ GeV}$ .

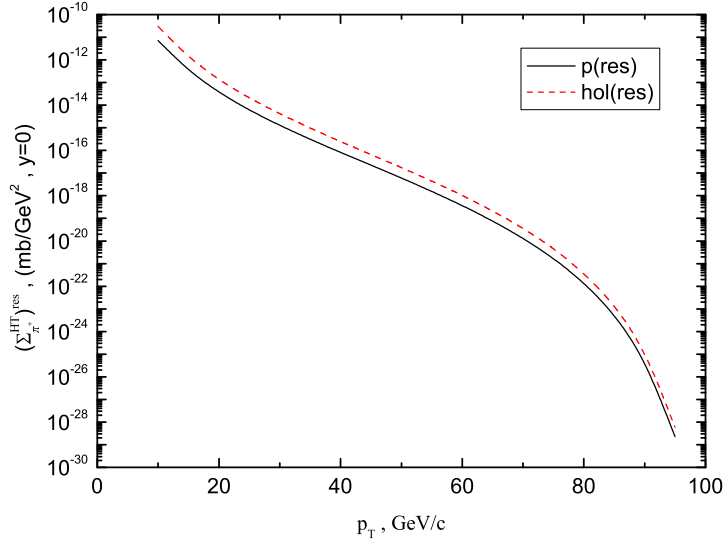


FIG. 11: Higher-twist  $\pi^+$  production cross section  $(\Sigma_{\pi^+}^{HT})^{res}$  as a function of the  $p_T$  transverse momentum of the pion at the c.m.energy  $\sqrt{s} = 200 \text{ GeV}$ .

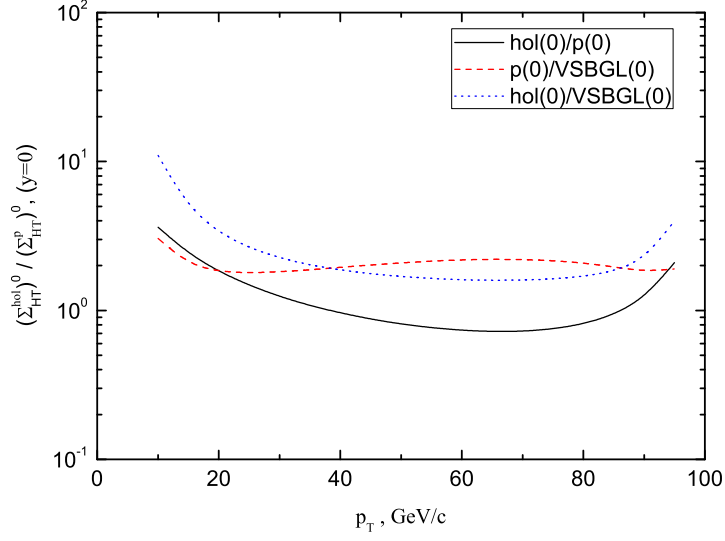


FIG. 12: Ratio  $(\Sigma_{HT}^{hol})^0 / (\Sigma_{HT}^p)^0$ , as a function of the  $p_T$  transverse momentum of the pion at the c.m.energy  $\sqrt{s} = 200 \text{ GeV}$ .

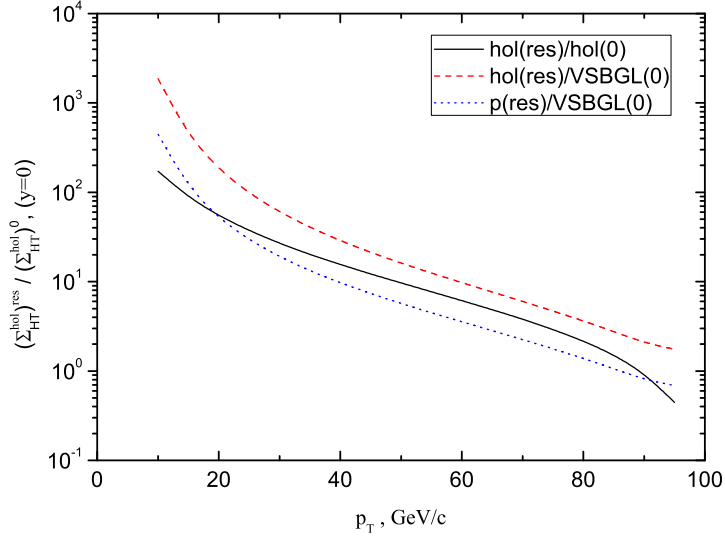


FIG. 13: Ratio  $(\Sigma_{HT}^{hol})^{res} / (\Sigma_{HT}^{hol})^0$ , as a function of the  $p_T$  transverse momentum of the pion at the c.m.energy  $\sqrt{s} = 200 \text{ GeV}$ .

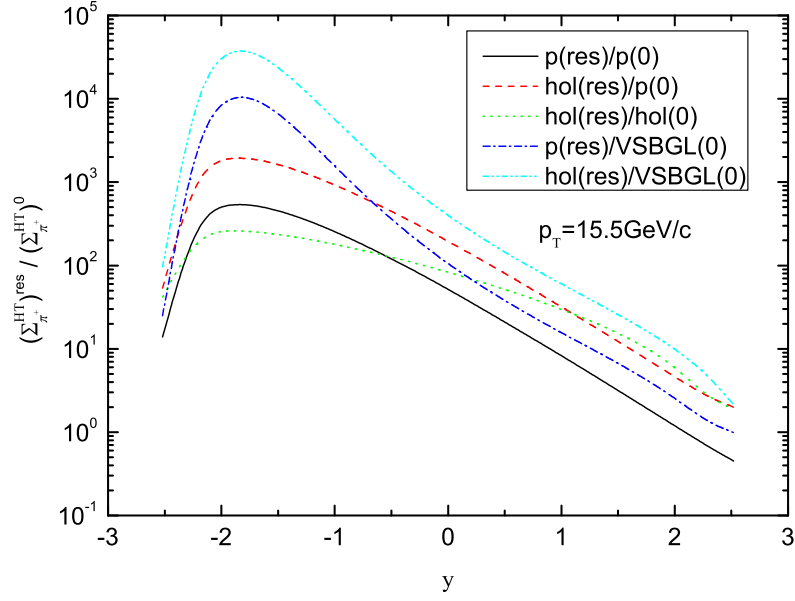


FIG. 14: Ratio  $(\Sigma_{\pi^+}^{HT})^{res}/(\Sigma_{\pi^+}^{HT})^0$ , as a function of the  $y$  rapidity of the pion at the transverse momentum of the pion  $p_T = 15.5 \text{ GeV}/c$ , at the c.m. energy  $\sqrt{s} = 200 \text{ GeV}$ .